Journal of Structural Biology **132,** 201–210 (2000)
doi:10.1006/jsbi.2000.4326, available online at http://www.idealibrary.com on IDEAL®

Statistical Evaluation of Colocalization Patterns in Immunogold Labeling Experiments

Anatoly A. Philimonenko,*,† Jiří Janáček,‡ and Pavel Hozák*,[1]

**Department of Cell Ultrastructure and Molecular Biology, Institute of Experimental Medicine, and ‡Department of Biomathematics, Institute of Physiology, Academy of Sciences of the Czech Republic, Prague, Czech Republic; and †Department of Evolutionary Animal Genetics, Institute of Cytology and Genetics, Siberian Division, Academy of Sciences of Russia, Novosibirsk, Russia*

Received September 16, 2000, and in revised form December 8, 2000

The ultrastructural localization of various antigens in a cell using antibodies conjugated to gold particles is a powerful instrument in biological research. However, statistical or stereological tools for testing the observed patterns for significant clustering or colocalization are missing. The paper presents a method for the quantitative analysis of single or multiple immunogold labeling patterns using interpoint distances and tests the method using experimental data. The clustering or colocalization of gold particles was detected using various characteristics of the distribution of distances between them. Pair correlation and cross-correlation functions were used for exploratory analysis; second order reduced *K* (or cross-*K*) functions were used for testing the statistical significance of observed events. Confidence intervals of function values were estimated by Monte Carlo simulations of the Poisson process for independent particles, and results were visualized in histograms. Furthermore, a suitability of *K* functions modified by censoring or weighting was tested. The reliability of the method was assessed by evaluating the labeling patterns of nascent DNA and several nuclear proteins with known functions in replication foci of HeLa cells. The results demonstrate that the method is a powerful tool in biological investigations for testing the statistical significance of observed clustering or colocalization patterns in immunogold labeling experiments. © 2000 Academic Press

Key Words: **cluster; colocalization; DNA replication; immunogold labeling; pattern analysis; stereology; ultrastructure.**

INTRODUCTION

Immunogold labeling is a specific and sensitive tool for detection of various antigens in biological samples. Usually, the immunogold detection is performed on ultrathin sections less than 100 nm thick. When a given cell structure contains a marker protein, immunogold labeling can be used for delineating this structure by observing spatial variations in labeling density. In a more complicated system, double immunogold labeling using gold particles of two sizes can be used for an assessment of spatial relationships, colocalization, or mutual inhibition (exclusion) of two kinds of structures. Unfortunately, appropriate statistical or stereological tools that would allow a biologist to test the significance of the observed patterns (clustering or colocalization, in particular) are missing. The aim of this paper therefore was to develop a suitable method for quantitative analysis of single or multiple immunogold labeling patterns using interpoint distances and to test the method using experimental data.

Methods using the distribution of interpoint distances (Ripley, 1980) can be used for testing the randomness of spatial patterns of one kind of label and the deviations of the spatial distribution of points from randomness: local increase (clustering) or local decrease (inhibition) in density of the label (e.g., in single immunogold labeling experiments). These methods can also be used for testing the independence of two types of labels and their deviation from independence: colocalization or mutual inhibition of the labels (e.g., in double immunogold labeling experiments). A clustering then causes a relative increase, while inhibition causes a relative decrease in the number of shorter interpoint distances when compared with a totally random process. Similarly, colocalization causes a relative increase, while inhibition causes a relative decrease in the number of shorter interpoint distances with respect to mutu-

[1] To whom correspondence should be addressed at Institute of Experimental Medicine, Department of Cell Ultrastructure and Molecular Biology, Vídenská 1083, 142 20 Prague 4-Krc, Czech Republic. Fax: +420(2) 475-22-19. E-mail: hozak@biomed.cas.cz.

1047-8477/00 $35.00

ally independent processes. In other words, a clustering causes an increase in the density of labels of one type in the vicinity of a typical label of the same type. Colocalization of two types of labels causes an increase of the density of labels of one type in the vicinity of a typical label of the other type. In order to analyze such spatial relationships of events, spatial statistics uses functions characterizing the density of events (i.e., particles) as a function of the distance from a typical event (Ripley, 1980; Stoyan *et al.*, 1995). For the analysis of clusters of particles of the same type, the pair correlation function (PCF) and the second reduced moment function (*K* function) were evaluated. In order to analyze the colocalization of particles, the pair cross-correlation function (PCCF) and the second reduced moment (or cross-*K*) function are used. In order to prove that the observed deviations from total randomness are significant, values of confidence intervals of the two functions were calculated by a method based on the Monte Carlo simulations.

Sometimes, depending on the type of immunogold technique used, there is more than one gold particle per labeled site, which may be erroneously detected as the clustering of particles. On the other hand, in some cases the size of immunoglobulin molecules prevents simultaneous detection of extremely close labeling sites that can result in short-range regularity or inhibition of particles (Glasbey and Roberts, 1997). Such specific properties of immunogold labeling require modifications of methods using interpoint distances. We modified them by an artificial censoring of short distances at which the effects mentioned above prevail.

As a biological model we have used DNA replication that takes place in cell nuclei in foci scattered throughout the nucleoplasm (Nakamura *et al.*, 1986; Nakayasu and Berezney, 1989; Hozák *et al.*, 1993). Immunogold labeling patterns of nascent DNA and of several nuclear proteins with known functions were investigated in replicating foci of synchronized mid-S-phase HeLa cells. The results proved that the method described can generally be used as a powerful tool in biological investigations requiring statistical analysis of immunogold clustering or colocalization patterns.

MATERIALS AND METHODS

Cell Culture and Synchronization

A suspension of HeLa cells was grown in Eagle's medium (S-MEM) (Sigma, St. Louis, MO) supplemented with 5% fetal calf serum (Sigma) at 37°C on rotamix. They were then synchronized using thymidine block in S-phase (2.5 mM thymidine, 22 h; Jackson and Cook, 1986), followed by a nocodazole block in mitosis using 20 ng/ml nocodazole (Sigma) for 8 h. Cells were then washed carefully and regrown in fresh medium. Samples were taken (about 5×10^6 cells per sample) 14 h after release from mitosis; this corresponds to mid-S-phase, as shown previously (Hozák *et al.*, 1994).

DNA Replication in Permeabilized Cells

Synchronized cells were spun down, washed twice in phosphate-buffered saline (PBS), permeabilized with saponin (0.1 mg/ml; Sigma) in "physiological" buffer (PB; Jackson *et al.*, 1988) for 3 min at 0°C, and washed in two changes of PB. PB (pH 7.4) contains 22 mM Na^+, 130 mM K^+, 1 mM Mg^{2+}, <0.3 μM free Ca^{2+}, 67 mM Cl^-, 65 mM CH_3COO^-, 11 mM phosphate, 1 mM ATP, 1 mM dithiothreitol, and 0.1 mM phenylmethylsulphonyl fluoride (PMSF). A prewarmed replication mix (10× concentrate) was added to permeabilized cells to give final concentrations of 100 μM CTP, UTP, and GTP, 250 μM dCTP, dATP, and dGTP, plus 100 μM biotin-16–dUTP (Boehringer Mannheim, Mannheim, Germany) and 2.15 mM $MgCl_2$. After 15 min at 33°C the reaction was stopped with 10 vol of ice-cold PB.

Antibodies

Monoclonal mouse antibodies to DNA polymerase α (SJK 287(1); Bensch *et al.*, 1982) and to hnRNP C1/C2 (clone 4F4; Choi and Dreyfuss, 1984) and polyclonal rabbit antibodies to nucleolar phosphoprotein Nopp 140 (Meier and Blobel, 1992) were used.

Electron Microscopy and Evaluation of Images

Following DNA replication in permeabilized HeLa cells, the cells were fixed for 30 min at 0°C in 3% paraformaldehyde and 0.1% glutaraldehyde in Sörensen buffer (0.1 M sodium/potassium phosphate buffer, pH 7.3; SB), washed in two changes of SB (10 min each), and resuspended in 1% low-melting-point agarose (Sigma) in SB at 37°C. Cells were then spun down and the pellet was cut into small pieces. The pieces were dehydrated in a series of ethanol solutions with increasing concentration of ethanol. The ethanol was then replaced in two steps by LR White resin (Polysciences Inc., Warrington, PA), and the resin was polymerized for 5 days at −20°C under UV light. After cutting 80-nm sections, nonspecific labeling was blocked by preincubation with 10% normal goat serum (British BioCell Int., Ltd., Cardiff, UK), 1% BSA, and 0.1% Tween 20 in PBS for 30 min at room temperature. For double immunogold labeling experiments the sections were incubated with primary antibodies against appropriate antigens (2–10 μg/ml), washed three times in PBT (0.005% Tween 20 in PBS), incubated with 5-nm-gold-conjugated goat antibodies to mouse or rabbit IgG and with 10-nm-gold-conjugated goat antibodies to biotin (British BioCell Int., Ltd.), washed again twice in PBT, then twice in bidistilled water, and air-dried. Finally, sections were contrasted with a saturated solution of uranyl acetate in water (4 min) and observed in a Philips CM100 electron microscope (Philips, Einthoven, Holland) equipped with a CCD camera (Model 673, GATAN, U.S.A.). Control incubations without a primary antibody proved that the signal was highly specific. For further statistical analysis of colocalization patterns, about 50 random digital electron microscope images of nuclear sections per each experimental group were taken. Each experimental group corresponded to one experiment in which biotin-labeled nascent DNA was colocalized with one of the proteins of interest. *XY* coordinates of all gold particles were recorded using a macro developed for LUCIA image-processing software (Laboratory Imaging Ltd., Prague, Czech Republic).

Identification of Colocalization Patterns

In order to analyze the clustering of particles, the second reduced moment *K* function and the PCF were used (Stoyan *et al.*, 1995). The *K* function is the number of gold particles (or points) at distances shorter than a given distance from a typical particle

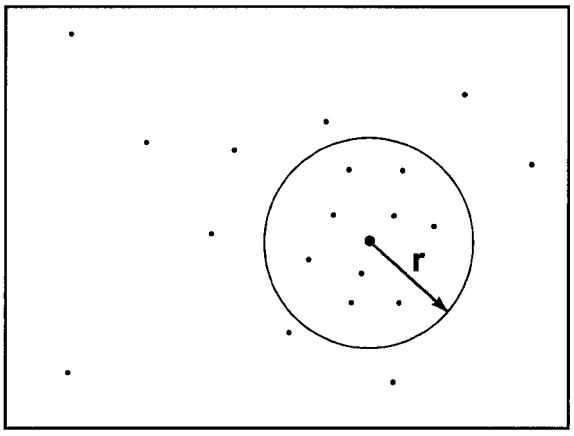

FIG. 1. A graphical representation of the evaluation of *K* and cross-*K* functions. The *K* function allows one to evaluate the clustering of the particles of one type. The *K* function is the ratio of the number of gold particles (points) at distances shorter than a given distance *r* (i.e., the points which are inside the circle with the radius *r*) from a typical particle of the same type (large point in the center of the circle) to the average density of these particles (here—the total number of particles in the frame divided by the area of this frame). In the case of the cross-*K* function, the large point in the center of the circle is a typical particle of the second type, while the remaining points are the particles of the first type. The cross-*K* function allows one to evaluate the colocalization of two types of particles, and it equals the number of gold particles of the first type at distances shorter than a given distance from a typical particle of the second type divided by the average density of the particles of the first type.

divided by the average density of these particles (see Fig. 1). PCF is a ratio of the density of gold particles at a given distance from a typical particle to the average density of these particles. Thus it is in principle possible to obtain PCF from the *K* function by differentiation using the formula (Stoyan *et al.*, 1995)

$$\mathrm{PCF}(r) = \frac{1}{2\pi r}\frac{dK(r)}{dr}. \qquad (1)$$

The clustering causes an increase in the density of particles in the neighborhood of a typical particle and, therefore, an increase of the values of both the PCF and the *K* function. In order to analyze the colocalization, we used the cross-*K* function, i.e., the number of gold particles of the first type at distances shorter than a given distance from a typical particle of the second type divided by the average density of the particles of the first type (see Fig. 1). Similarly, we evaluated the PCCF as the ratio of the density of particles of the first type at the given distance from a typical particle of the second type to the average density of the particles of the first type. For the PCCF and the cross-*K* function the same relationship holds as that for the PCF and the *K* function (see formula above). The pair (cross)correlation functions are useful for exploratory analysis, while the *K* functions for statistical testing (Stoyan *et al.*, 1995). The exploratory analysis provides one with information if the clustering or colocalization is present and, if so, at what distances. This information can then be used in more detailed confirmatory analysis, especially for setting the appropriate ranges of distances that are to be tested. An inappropriately low range might cause an omission of significant clustering/colocalization at distances longer than set. In contrast, too high a range much larger than the typical size of clusters would cause a low spatial resolution of the test.

The above functions were calculated from pooled data from all images of nucleoplasm in each experimental group. Let N be the number of images of size $a \times b$. Let $n_{1,i}$ be the number of 10-nm particles in the image number i; similarly, let $n_{2,i}$ be the number of 5-nm particles in image number i; $i = 1 \cdots N$. Then density of jth labeling λ_j ($j = 1$ or $j = 2$ in the case of 10- or 5-nm gold particles, respectively) can be estimated as

$$\widehat{\lambda_j} = \frac{1}{NA}\sum_{i=1}^{N} n_{j,i}, \qquad (2)$$

where $A = ab$ is the area of one image. The functions were then estimated by sampling distances $d(x, y)$ between points x and y which correspond to pairs of particles in each window (one window corresponds to one image). However, the sampling of long distances is negatively biased, because the probability that one particle from the pair is situated outside of the window (image) increases with an increase of the distance between gold particles (Fig. 2A). This negative bias, called boundary effect, may be corrected using the geometric covariogram γ of the window (Ripley, 1988). In order to obtain this parameter, a rectangle with sides a and b (which corresponds to an image) was shifted by

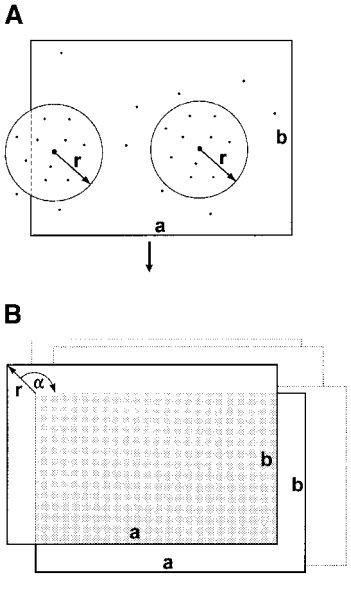

FIG. 2. Correction of the boundary effect using geometric window covariogram. (A) The probability that one gold particle from the pair is situated outside of the window (image) increases with an increase of the distance r at which the colocalization/clustering is evaluated. (B) This negative influence, called the boundary effect, may be corrected using the geometric covariogram γ of the window (see Eqs. 3 and 4 under Materials and Methods; Ripley, 1988). To obtain this parameter, a rectangle with sides a and b is shifted by distance r in all directions (α angle ranges from 0 to 2π), and the areas of intersections between the original rectangle and the shifted ones (gray-colored area) were measured. The geometric window covariogram $\gamma(r)$ equals the average area of the intersections; a and b equal the length of the sides of the window.

distance r in all directions from 0 to 2π, and the area of intersections between the original rectangle and the shifted ones was evaluated (see Fig. 2B). The average area of intersections which corresponds to the geometric window covariogram $\gamma(r)$ can be then calculated for $r < \min(a, b)$ accordingly:

$$\gamma(r) = a \cdot b - \frac{2}{\pi} \cdot (a + b) \cdot r + \frac{1}{\pi} \cdot r^2. \tag{3}$$

Let $X_{j,i}$ be a set of labels of type j in ith image and let $r'' > r' \geq 0$. Then the bottom-censored K function for points x and y will be estimated similarly to the classical K function (in the case of $r' = 0$, Ripley, 1980):

$$\widehat{K}_j(r', r'') = \frac{1}{N \widehat{\lambda}_j^2} \sum_{i=1}^{N} \sum_{\substack{x,y \in X_{j,i} \\ x \neq y}} \frac{1[r' \leq d(x, y) < r'']}{\gamma(d(x, y))}. \tag{4}$$

A graphical representation of the bottom-censored K function evaluation is given in Fig. 3. Also, the bottom-censored cross-K function for 10-nm particles ($j = 1$) and 5-nm particles ($j = 2$) will be estimated as

$$\widehat{K}_{1,2}(r', r'') = \frac{1}{N \widehat{\lambda}_1 \widehat{\lambda}_2} \sum_{i=1}^{N} \sum_{\substack{x \in X_{1,i} \\ y \in X_{2,i}}} \frac{1[r' \leq d(x, y) < r'']}{\gamma(d(x, y))}. \tag{5}$$

Condition $r' \leq d(x, y) < r''$ means that point y is lying inside the sector created with circles of the radii r' and r'' which have centers in the point x (see Fig. 3). Thus the expression "1[condition]" is for indicator function; it has value 1 if the condition is fulfilled and 0 otherwise. Similarly, we estimate K_j^{-1} and $K_{1,2}^{-1}$, which are the integrals (from r' to r'') of pair correlation and pair cross-correlation functions (PCF and PCCF, Stoyan *et al.*, 1995), respectively, as

$$\widehat{K}_j^{-1}(r', r'') = \frac{1}{2\pi N \widehat{\lambda}_j^2} \sum_{i=1}^{N} \sum_{\substack{x,y \in X_{j,i} \\ x \neq y}} \frac{1[r' \leq d(x, y) < r'']}{d(x, y) \cdot \gamma(d(x, y))} \tag{6}$$

$$\widehat{K}_{1,2}^{-1}(r', r'') = \frac{1}{2\pi N \widehat{\lambda}_1 \widehat{\lambda}_2} \sum_{i=1}^{N} \sum_{\substack{x \in X_{1,i} \\ y \in X_{2,i}}} \frac{1[r' \leq d(x, y) < r'']}{d(x, y) \cdot \gamma(d(x, y))}. \tag{7}$$

Histograms of PCFs and of PCCFs with delimiting points r_0, r_1, $r_2 \cdots$ defined as 0, dr, $2dr \cdots$ were constructed using estimates of mean values of PCF and PCCF (which correspond to the heights of histogram bars). These mean values were estimated on the intervals (r_i, r_{i+1}) and defined as

$$\widehat{K}_j^{-1}(r_i, r_{i+1})/(r_{i+1} - r_i) \text{ and } \widehat{K}_{1,2}^{-1}(r_i, r_{i+1})/(r_{i+1} - r_i), \tag{8}$$

respectively. The width of histogram bars was calculated from the number of images and particle density for PCF histograms as

$$dr = \frac{0.1\sqrt{3}}{\sqrt[4]{N\lambda_j^2}} \tag{9}$$

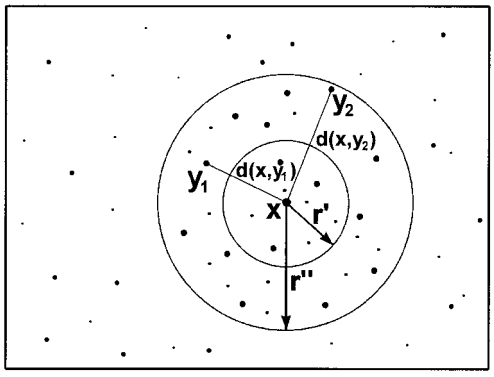

FIG. 3. Illustration for the estimation of the bottom-censored K and cross-K functions for particles of one or two types, respectively (see also Eqs. 3–5 under Materials and Methods). Let x, y_1, and y_2 be the particles of the same type. In both cases $d(x, y_1)$ and $d(x, y_2)$ (distances between points x and y_1 and x and y_2) fulfil the condition $r' \leq d(x, y) < r''$. Any point y_n will be taken into account for the evaluation of the bottom-censored K function only if it is lying inside the sector, delimited by the circles of the radii r' and r'' with a common center in the point x. In the case of the evaluation of the bottom-censored cross-K function, the point x will be a gold particle of one type, while points y_n will be the gold particles of the other type. Thus the colocalization/clustering at a specified range of distances can be evaluated by comparing the densities of particles y_n inside the sector to the average density of these particles.

and also for PCCF histograms as

$$dr = \frac{0.1\sqrt{3}}{\sqrt[4]{2N\lambda_1\lambda_2}}. \tag{10}$$

Monte Carlo estimates (Barnard, 1963) of two-sided 95% confidence intervals for histogram bar heights and one-sided 1 and 5% tests for clustering or colocalization were carried out using 999 simulations of N realizations (N is equal to the number of evaluated images) of the binomial process with number of simulated points equal to the observed points numbers $n_{j,i}$. The characteristics of the tests (values of $K(r, r')$ functions which were defined above) were calculated. For the estimation of histogram confidence intervals the calculated 25th extreme value of the bar height was used as critical value for two-sided 5% tests. Similarly, calculated critical values were used for verifying the clustering and/or colocalization of the particles: for the one-sided tests the 50th value from the maximum was used at the 5% confidence level, and the 10th value from the maximum at the 1% confidence level.

RESULTS

Examples of electron micrographs of HeLa cells nucleoplasm labeled with gold-conjugated antibodies for DNA polymerase α, hnRNP C1/C2, Nopp 140, and nascent DNA are presented in Figs. 4A–4C, respectively. The results were more predictable for DNA polymerase α (strong colocalization with nascent DNA) and Nopp 140 (absence of colocalization with nascent DNA), while for hnRNP C1/C2 they

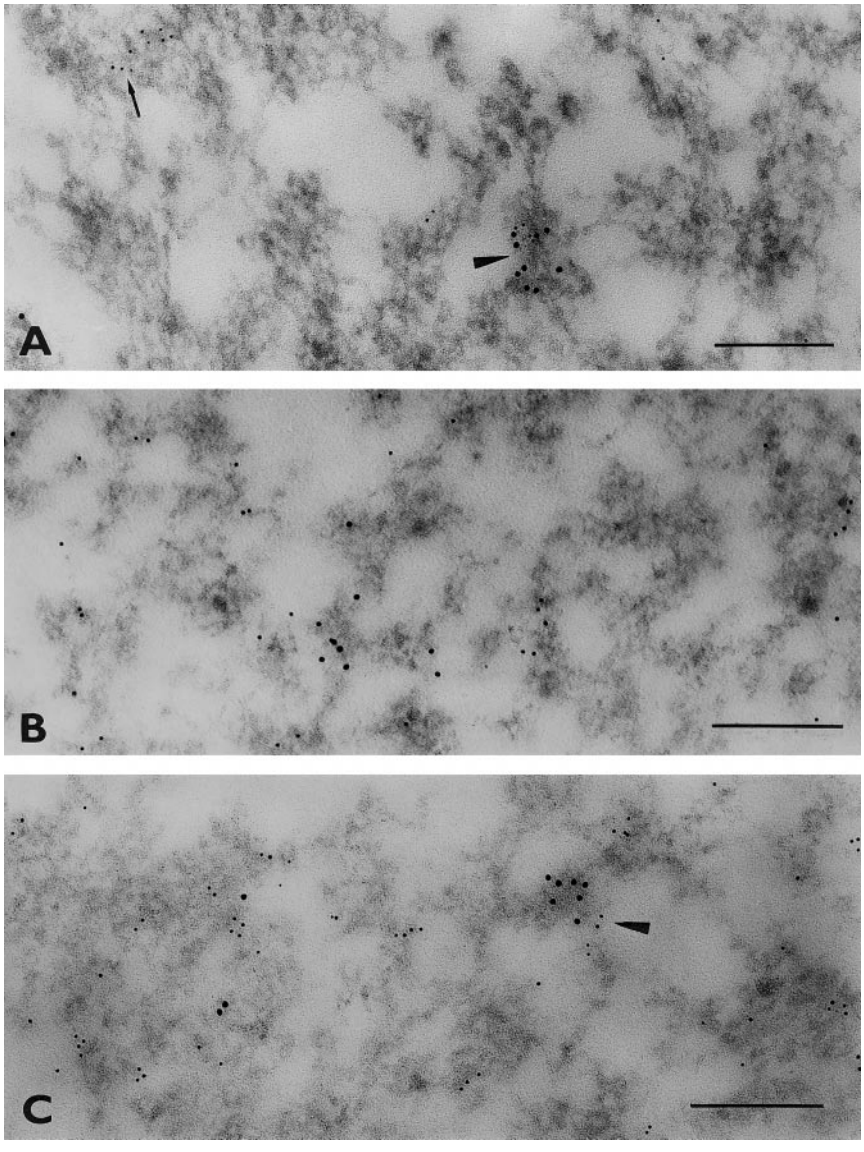

FIG. 4. Electron micrographs of HeLa cells. (A) Double immunogold labeling of DNA polymerase α (5-nm gold particles) and biotin-labeled nascent DNA (10-nm gold particles). Clusters of DNA polymerase α are detectable separately (arrow) or intermingled with clusters of labeled nascent DNA (arrowhead). (B) Double immunogold labeling of hnRNP C1/C2 (5-nm gold particles) and nascent DNA (10-nm gold particles). Colocalization of hnRNP C1/C2 and nascent DNA is not obvious by visual inspection. (C) Double immunogold labeling of Nopp 140 (5-nm gold particles) and nascent DNA (10-nm gold particles). Nopp 140 is detected throughout the nucleoplasm, sometimes close to labeled nascent DNA (arrowhead). Bars, 200 nm.

were not so obvious. In order to evaluate the mutual localization of gold particles we calculated the total number and XY coordinates of all gold particles in each image (for more details see Materials and Methods). Densities of both types of labeling are given in Table I. The labeling density of 5-nm gold particles was similar in DNA polymerase α and Nopp 140 experimental groups, while for the hnRNP C1/C2 it was higher. The density of 10-nm gold particles was similar in all three groups. This was expected, as the same anti-biotin antibodies and experimental conditions were used.

In order to evaluate clustering patterns of gold particles of each type, we used the PCF. Clustering is clearly visible in all types of samples (peaks of histograms in Figs. 5A and 5B for DNA polymerase α and nascent DNA, Figs. 6A and 6B for hnRNP C1/C2 and nascent DNA, and Figs. 7A and 7B for Nopp 140 and nascent DNA, respectively). The size of clusters is larger in the case of DNA polymerase α

TABLE I
Numerical Densities of 10-nm and 5-nm Gold Particles

Antigen	λ1	λ2
DNA polymerase α	15.1	32.5
hnRNP C1/C2	13.6	139.4
Nopp 140	18.7	38.0

Note. Double immunogold labeling was performed on ultrathin sections of cells in three independent experiments. The 10-nm gold particles conjugated to anti-biotin antibodies were used to detect nascent DNA (biotin) in all three experiments. Simultaneously, 5-nm gold particles were used for the detection of antibodies recognizing DNA polymerase α, hnRNP C1/C2, or Nopp 140 in each experiment, respectively. Numerical densities (number of particles/μm^2) of 10-nm (λ1) and 5-nm (λ2) gold particles were then estimated.

than in the case of hnRNP C1/C2 and Nopp 140 (compare Fig. 5A and Figs. 6A and 7A). For the evaluation of colocalization the PCCF was calculated. Colocalization with nascent DNA is highly significant in case of DNA polymerase α (Figs. 5C and 4A, arrowhead) and absent in the case of Nopp 140 (Fig. 7C). Colocalization of hnRNP C1/C2 with nascent DNA was detected (Fig. 6C); however, it was not so strong as that for DNA polymerase α and the distances at which colocalization occurs were shorter than those for DNA polymerase α (compare with Fig. 5C). Some comment is necessary here: the method allows detection of weak and not visually obvious colocalizations. For example, when we compare the electron microscopic micrographs showing the distribution of gold particles marking hnRNP C1/C2 and Nopp 140 relative to nascent DNA (see Figs. 4B and 4C), the observed patterns are very similar. Nevertheless, the *K* function clearly revealed a colocalization.

The finite size of immunoglobulin molecules is about 8–10 nm in the most extended state. Thus in cases when two antigens lie on the surface of a section closer than 20 nm one to another, the gold particles bound to antibodies can repulse. This inhibition at short distances (<20 nm) sometimes causes an obvious decrease in PCF and PCCF values in the interval 0–20 nm (see, e.g., Figs. 5C, 6C, and 7C).

Colocalization of two types of labels was also tested for different intervals of distances between gold particles using the *K* and K^{-1} functions described above. The intervals of distances between particles were 0–30, 30–100, 100–250, 0–100, and 30–250 nm. The method using the integral of cross-correlation function (K^{-1}, Table II) gave the same results (at 5 and 1% significance levels) for distances longer than 30 nm as the method using the bottom-censored cross-*K* function (Table III). This approach allows one to evaluate precisely the intervals of distances at which the colocalization/clustering occurs and then to make a conclusion about the size of clusters or underlying structures. For example, in our case the distances at which colocalization of the nascent DNA with DNA polymerase α occurs are larger than those of hnRNP C1/C2 (compare Figs. 5C and 6C). The accuracy of the determination of the size of structures/clusters depends on the length of each interval. However, a limitation exists: in extremely short intervals the number of gold particles inside of a particular interval will be insufficient for statistical analysis. Optimization of the intervals is therefore suggested.

DISCUSSION

We have developed an apparently powerful method for ultrastructural studies that allows one to

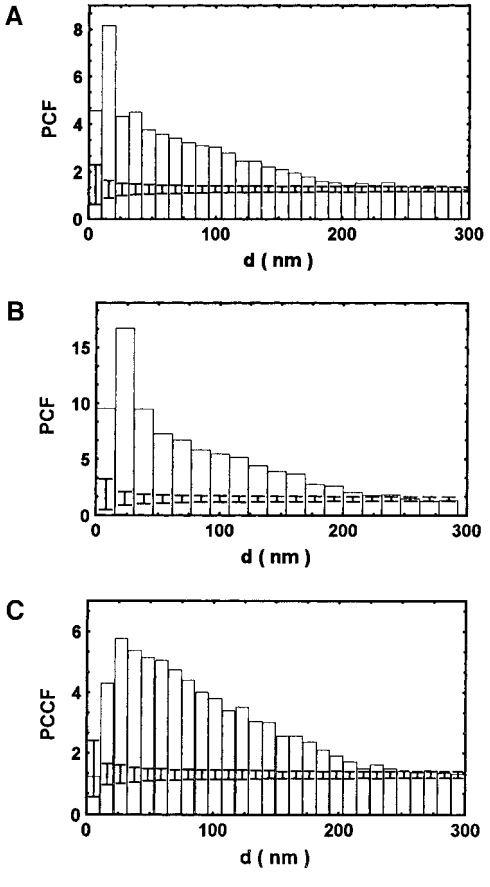

FIG. 5. Clustering and colocalization patterns of DNA polymerase α and nascent DNA. (A) Clustering of DNA polymerase α (5-nm gold particles) is clearly visible in the interval of distances between particles of 20–150 nm (note that the PCF in this interval is significantly higher than 1). (B) Clustering of nascent DNA (10-nm gold particles) occurs in the interval of 20–150 nm. (C) Colocalization of DNA polymerase α and nascent DNA. The 5% confidence intervals were obtained by Monte Carlo simulations of independent random processes. Both antigens strongly colocalize in the interval of 20–175 nm; the PCCF function reaches values well above 1.

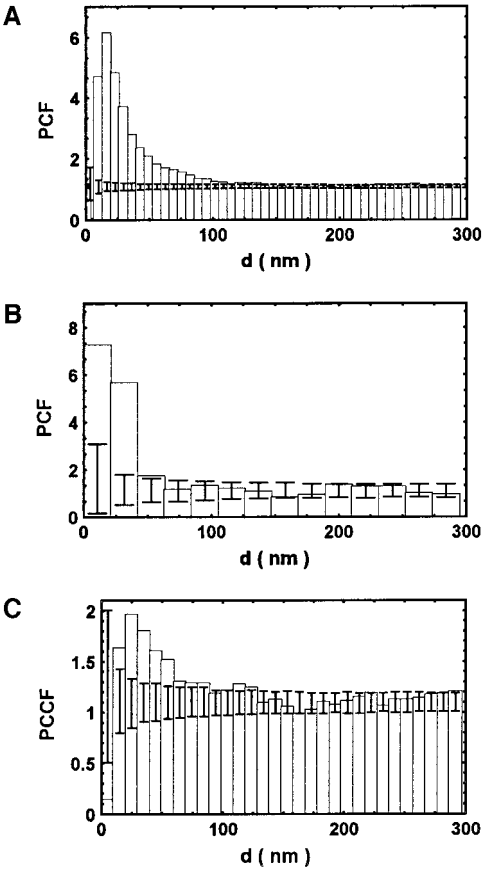

FIG. 6. Colocalization and clustering patterns of hnRNP C1/C2 and nascent DNA. (A) Clustering of hnRNP C1/C2 (5-nm gold particles) is clearly visible in the interval of distances between particles of 20–75 nm (note that the PCF in this interval is significantly higher than 1). (B) Clustering of nascent DNA (10-nm gold particles) occurs in the interval of 20–50 nm. (C) Colocalization of hnRNP C1/C2 and nascent DNA. The 5% confidence intervals were obtained by Monte Carlo simulations of independent random processes. Both antigens colocalize in the interval of 20–75 nm.

evaluate the colocalization and clustering of different antigens in biological samples. The method allows us to confirm or disregard a hypothesis on colocalization/clustering of antigens using rigorous statistical means.

Immunogold labeling, which is widely used for the detection of antigens in ultrastructural studies, is an example of the dense packing of points (gold particles). For this process, a decrease in the number of short interpoint distances (<20 nm) and a small increase in the number of distances about 30 nm (so-called short-range effects) are typical. This decrease in the number of short interpoint distances is caused by the physical size of antibodies (7–10 nm) to which the particles are attached. In opposition, a small increase in the number of distances around 20–30 nm can be caused by the accumulation of particles, which were "pushed" by the molecules of antibodies outward (Glasbey and Roberts, 1997). These short-range effects may complicate the statistical analysis of distances between gold particles. To overcome these problems, statistical analysis of interpoint distances was performed using a few modifications of classical second-order reduced K function (Ripley, 1980). Previously described $K(r)$ function (number of particles within a distance r from a typical particle divided by the average density of the particles; Ripley, 1980) was calculated from distances shorter than the specified distance r. We have developed a bottom-censored K function $K(r_1, r_2)$ calculated only from distances in the interval (r_1, r_2), which enables us to exclude the short-range effects caused by dense packing of anti-

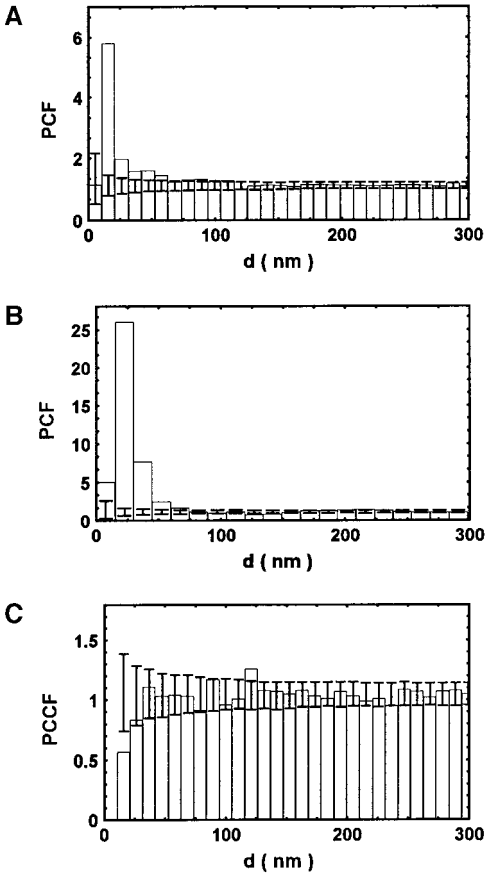

FIG. 7. Colocalization and clustering patterns of Nopp 140 and nascent DNA. (A) Clustering of Nopp 140 (5-nm gold particles) occurs in the interval of distances between particles of 20–50 nm (note that the PCF in this interval is significantly higher than 1). (B) Clustering of nascent DNA (10-nm gold particles) occurs in the interval of 20–50 nm. (C) Colocalization of Nopp 140 and nascent DNA. The 5% confidence intervals were obtained by Monte Carlo simulations of independent random processes. Antigens do not colocalize: the PCCF has no peak in any interval and is fluctuating around 1.

TABLE II

Experimental Values of the Integral of the Pair Cross-Correlation Function (K^{-1}) for Different Intervals of Distances between 5- and 10-nm Gold Particles Are Compared with K^{-1} Function Critical Values (*$P < 0.05$; **$P < 0.01$)

	Interval (nm)														
	0–30			30–100			100–250			0–100			30–250		
Antigens	K^{-1}	5%	1%	K^{-1}	5%	1%	K^{-1}	5%	1%	K^{-1}	5%	1%	K^{-1}	5%	1%
DNA polymerase α and nascent DNA	0.110**	0.049	0.056	0.333**	0.095	0.097	0.364**	0.200	0.203	0.443**	0.139	0.146	0.697**	0.293	0.295
hnRNP C1/C2 and nascent DNA	0.038	0.040	0.047	0.100**	0.081	0.082	0.169	0.170	0.171	0.138**	0.118	0.125	0.269**	0.248	0.251
Nopp 140 and nascent DNA	0.013	0.039	0.048	0.073	0.077	0.078	0.158	0.161	0.162	0.086	0.112	0.121	0.230	0.235	0.238

Note. The K^{-1} function was calculated in three independent double labeling experiments using antibodies against biotin (nascent DNA) and one of the antibodies raised against DNA polymerase α, hnRNP C1/C2 or Nopp 140.

bodies and to test for clustering or colocalization in the range of distances specified by the investigator. This can be achieved by setting r_1 and r_2 ($r_1 < r_2$) to any number within the range that is of interest in the particular experiment (in our case, 30–200 nm—the range of typical sizes of replication foci in cell nuclei; see Tables II and III). These results demonstrate again the strongest feature of the method: it allows us to evaluate the precise intervals at which the colocalization/clustering occurs and thus to form a conclusion about the size of clusters in relation to underlying structures.

We also calculated PCF and PCCF that can be derived from the K function (see Materials and Methods). They are equal to the ratios of the densities of gold particles at a given distance from a typical particle to the average densities of these particles. The PCF describes the clustering of single type particles, while the PCCF describes the colocalization of particles of two types.

Another modification of the standard Ripley's K functions was the transformation to K^{-1} functions, which are the integrals of PCF and PCCF. K^{-1} functions are calculated similarly to K functions, but weighting the sampled distances by the -1st power of these distances. The value of $K^{-1}(r_1, r_2)$ has an easy interpretation: we can detect deviations from randomness by comparing it directly to the difference of the diameters r_2 and r_1 ($r_2 - r_1$) because the mean value of $K^{-1}(r_1, r_2)$ for completely random point pattern is equal to $r_2 - r_1$. It is also used for graphical representation of the (cross)correlation functions. The integral of PCF or PCCF from r_1 to r_2 represents an area of the histogram bar for each interval of distances $r_2 - r_1$. This area can be easily calculated as the height of histogram bars representing the value of PCF or PCCF in the interval (r_1, r_2), while the width of the bars equals $r_2 - r_1$. In the case of single or multiple immunogold labeling, we recommend the use of the histogram representation as it demonstrates the characteristics of clustering and/or colocalization (characteristic distance

TABLE III

Experimental Values of the Bottom-Censored K Function for Different Intervals of Distances between 5- and 10-nm Gold Particles Are Compared with K Function Critical Values (*$P < 0.05$; **$P < 0.01$)

	Interval (nm)														
	0–30			30–100			100–250			0–100			30–250		
Antigens	K	5%	1%	K	5%	1%	K	5%	1%	K	5%	1%	K	5%	1%
DNA polymerase α and nascent DNA	0.013**	0.004	0.004	0.132**	0.039	0.040	0.370**	0.219	0.223	0.145**	0.043	0.043	0.501**	0.257	0.260
hnRNP C1/C2 and nascent DNA	0.005**	0.004	0.004	0.039**	0.033	0.033	0.185	0.187	0.189	0.044**	0.036	0.037	0.224**	0.218	0.221
Nopp 140 and nascent DNA	0.002	0.003	0.004	0.030	0.031	0.032	0.172	0.177	0.178	0.031	0.034	0.035	0.202	0.207	0.209

Note. The K function was calculated in three independent double labeling experiments, as described in the Table II legend.

and degree of clustering or colocalization) of gold particles in a clear and comprehensive manner. The confidence intervals of heights of the histogram bars allow the investigator to judge whether the deviations from randomness are statistically significant.

We also compared the ability of $K(r_1, r_2)$ and $K^{-1}(r_1, r_2)$ functions to assess the significance of differences between the observed and random distributions of gold particles. The numerical tests of significance based on bottom-censored $K(r_1, r_2)$ and $K^{-1}(r_1, r_2)$ functions gave nearly identical results; the differences between the two functions were present only for $r_1 = 0$, where the $K^{-1}(r_1, r_2)$ function may have large variance. Therefore, in agreement with Stoyan (1995), we recommend the use of the K^{-1} function, i.e., the integrals of (cross) correlation functions, to construct histograms for exploratory analysis, and $K(r_1, r_2)$ functions for testing the significance of colocalization/clustering.

The exclusion of the short-range effects by setting r_1 to 30 nm (the approximate distance up to which interactions between antibodies carrying gold particles take place) had no effect on colocalization/clustering significance testing by original Ripley's (cross) $K(r) = K(0, r)$ function performed on data presented in this article (compare corresponding columns in Table III). However, in other cases (data not shown) this influence was present and it was necessary to exclude this 0- to 30-nm interval (as we cannot be sure about the nature of interactions between antibodies at this interval). On the other hand, this interval can be reduced by using a single-step immunogold labeling procedure when gold particles are conjugated directly with a primary antibody.

When random images of any area (in our case the nucleoplasm) are used, it is necessary to pay attention to the boundary effect, as the sampling of long distances is negatively biased due to the limited size of the window. The correction for the boundary effect applied to the calculations of both K and K^{-1} functions (which is described under Materials and Methods) is correct only for a random position of the observation window. However, the error caused by the violation of randomness is assumed to be negligible for the distances of interest we have used, as they are much shorter than the window size.

The K and K^{-1} functions give us the opportunity to evaluate the clustering of different antigens in biological samples. In our case, these functions were used in order to obtain new data about clustering characteristics of different antigens in the volume of the nucleus. For instance, the comparison of DNA polymerase α clustering with the clustering pattern of hnRNP C1/C2 or Nopp 140 demonstrated variations in the sizes of the clusters. The distances at which clustering occurs are longer in the case of DNA polymerase α than those of hnRNP C1/C2 and Nopp 140. Apparently, this shows that the molecules of DNA polymerase α occupy structures with larger volumes in the space of the nucleus than the other two antigens.

The method has very good reliability for the detection of colocalization, as we have shown in our testing system. For example, the results of experiments obtained for DNA polymerase α and Nopp 140 fit very well to the expected patterns. DNA polymerase α, the principal replicative DNA polymerase in actively multiplying eucaryotic cells (Salas *et al.*, 1999), demonstrates a strong colocalization with nascent DNA over the range of distances that corresponds to the known size of replication foci (for a review, see Hughes *et al.*, 1995). In contrast, the nucleolar protein Nopp 140 (Meier and Blobel, 1992), which is not expected to be involved in DNA replication, did not colocalize with nascent DNA.

On the other side, the results of the statistical evaluation of colocalization patterns proved that the method presented is capable of providing new and even unexpected information of biological significance. Significant colocalization of hnRNP C1/C2, which is known to be involved in mRNA processing (for a review see, e.g., Dreyfuss *et al.*, 1993), with nascent DNA detected in our experiments serves as an example. Although there are some hints in the literature on colocalization of transcription and replication processes in the cell nucleus (Hassan and Cook, 1994), the discussion of the possible involvement of this hnRNP in the process of DNA replication is beyond the scope of this paper. Nevertheless, such colocalization of proteins with known functions with other (unexpected) processes or structures can demonstrate certain higher levels of "colocalization" of those processes in the 3-D organization of the cell nucleus. However, some caution is necessary: a colocalization of two structures does not have to mean a functional connection. It can be caused for example by simultaneous exclusion from a part of the reference space, e.g., from chromosomal zones.

What should be the practical recommendations for researchers? First, the limit of the distance r should be less than the shorter side of the window. Second, the pair correlation and cross-correlation functions should be used for exploratory analysis; in other words, these functions presented in histograms inform the user if there is any clustering or colocalization and at what distances. As a consequence, the user can estimate the upper limit of r for the K and K^{-1} functions (respectively, d in histograms). This should prevent one from an omission of clustering or colocalization at shorter distances. Third, the interactions of gold particles, antibodies, and the antigen

can vary at very short distances depending on antibody type, gold particle size, direct or indirect immunogold labeling, etc. The user should therefore consider very carefully the interpretation of results at distances shorter than 30 nm. Furthermore, the method is not appropriate for the detection of clustering or colocalization for distances shorter than the maximal size of the immunogold, i.e., about 15 nm for 5-nm gold particles and 25 nm for 10-nm gold particles. Fourth, the densities of gold labeling used for testing the method in this article appear to be entirely sufficient for the efficient detection of clustering or colocalization patterns. Much lower densities can be also used; however, this needs to be compensated by a higher number of evaluated windows.

In conclusion, the experiments presented confirmed the ability of the novel approach to provide new data of biological significance. The K^{-1} function gives an easy visual impression about the presence of clustering/colocalization, while the K function provides more detailed statistical evaluation of the data. The method described can widen biological applications of ultrastructural immunogold labeling techniques especially in investigations dealing with biological functions of different cell structures. A computer program named "Gold" was written. The program evaluates the described statistical features and also produces graphical output in the form of histograms identical to those presented in the paper. It runs under Windows 95/98/NT/2000 and can be obtained from the authors without charge upon request or downloaded directly from http://uemweb.biomed.cas.cz/hozak/gold.htm.

We thank Dr. Ivan Saxl and Dr. Lucie Kubinova for their helpful comments. We thank the Grant Agency of the Czech Republic (Grant Reg. No. 304/98/1035), the Grant Agency of the Academy of Sciences of the Czech Republic (Grant Reg. No. A5039701), and The Wellcome Trust (UK) for support. This article is devoted to the memory of Dr. Ivan Krekule, whose valuable comments helped to create the method described.

REFERENCES

Barnard, G. (1963) Contribution to discussion of Bartlett, *J. Roy. Stat. Soc.* **B25,** 294.

Bensch, K. G., Tanaka, S., Hu, S. Z., Wang, T. S., and Korn, D. (1982) Intracellular localization of human DNA polymerase alpha with monoclonal antibodies, *J. Biol. Chem.* **257,** 8391–8396.

Choi, Y. D., and Dreyfuss, G. (1984) Monoclonal antibody characterization of the C proteins of heterogeneous nuclear ribonucleoprotein complexes in vertebrate cells, *J. Cell Biol.* **99,** 1997–2004.

Dreyfuss, G., Matunis, M. J., Pinol-Roma, S., and Burd, C. G. (1993) hnRNP proteins and the biogenesis of mRNA, *Annu. Rev. Biochem.* **62,** 289–321.

Glasbey, C. A., and Roberts, I. M. (1997) Statistical analysis of the distribution of gold particles over antigen sites after immunogold labeling, *J. Microsc.* **186,** 258–262.

Hassan, A. B., and Cook, P. R. (1994) Does transcription by RNA polymerase play a direct role in the initiation of replication? *J. Cell Sci.* **107,** 1381–1387.

Hozák, P., Hassan, A. B., Jackson, D. A., and Cook, P. R. (1993) Visualization of replication factories attached to a nucleoskeleton, *Cell* **73,** 361–373.

Hozák, P., Jackson, D. A., and Cook, P. R. (1994) Replication factories and nuclear bodies: The ultrastructural characterization of replication sites during the cell cycle, *J. Cell Sci.* **107,** 2191–2202.

Hughes, T. A., Pombo, A., McManus, J., Hozák, P., Jackson, D. A., and Cook, P. R. (1995) On the structure of replication and transcription factories, *J. Cell Sci.* **19**(Suppl.), 59–65.

Jackson, D. A., and Cook, P. R. (1986) A cell cycle dependent DNA polymerase activity that replicates intact DNA in chromatin, *J. Mol. Biol.* **192,** 65–76.

Jackson, D. A., Yuan, J., and Cook, P. R. (1988) A gentle method for preparing cyto- and nucleo-skeletons and associated chromatin, *J. Cell Sci.* **90,** 365–378.

Meier, U. T., and Blobel, G. (1992) Nopp 140 shuttles on tracks between nucleolus and cytoplasm, *Cell* **70,** 127–138.

Nakamura, H., Morita, T., and Sato, C. (1986) Structural organization of replicon domains during DNA synthetic phase in the mammalian nucleus, *Exp. Cell Res.* **165,** 291–297.

Nakayasu, H., and Berezney, R. (1989) Mapping replication sites in the eucaryotic cell nucleus, *J. Cell Biol.* **108,** 1–11.

Ripley, B. D. (1980) Spatial Statistics, Wiley, New York.

Ripley, B. D. (1988) Statistical Inference for Spatial Processes, Cambridge Univ. Press, Cambridge.

Salas, M., Miller, T. J., Leis, J., and DePamphilis, M. L. (1999) Mechanisms for priming DNA synthesis, *in* Concepts in Eucaryotic DNA Replication, Cold Spring Harbor Laboratory Press, Cold Spring Harbor, NY.

Stoyan, D., Kendall, W. S., and Mecke, J. (1995) Stochastic Geometry and Its Applications, Wiley, Chichester.